analytical chemistry

pubs.acs.org/ac Article

Intuitive Model of Surface Modification Induced by Cluster Ion Beams

Dawid Maciążek, Micha Kański, and Zbigniew Postawa*

Cite This: *Anal. Chem.* 2020, 92, 7349−7353 Read Online

ACCESS | Metrics & More | Article Recommendations

ABSTRACT: Topography development is one of the main factors limiting the quality of depth profiles during depth profiling experiments. One possible source of topography development is the formation of self-organized patterns due to cluster ion beam irradiation. In this work, we propose a simple model that can intuitively explain this phenomenon in terms of impact-induced mass transfer. By coupling our model with molecular dynamics simulations, we can predict the critical incidence angle, which separates the smoothening and roughening regimes. The results are in quantitative agreement with experiments. It is observed that the problems arising from topography development during depth profiling with cluster projectiles can be mitigated by reducing the beam incidence angle with respect to the surface normal or increasing its kinetic energy.

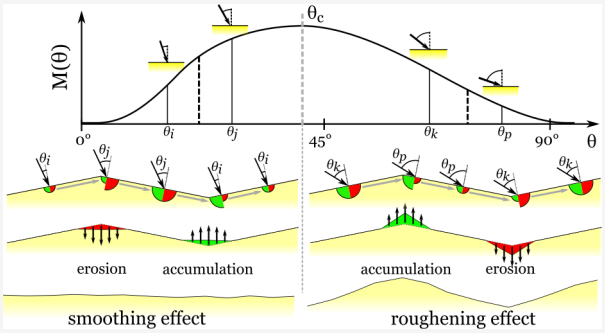

Surface-sensitive techniques such as Secondary Ion Mass Spectrometry (SIMS), X-ray Photoelectron Spectroscopy (XPS), and Auger Electron Spectroscopy (AES) combined with ion-induced material removal can be used to create spatial maps of the chemical composition of materials in a process called depth profiling. This approach has been successfully applied to many systems both inorganic and organic.[1−3] The main problem of depth profile acquisition is the degradation of resolution with a time of analysis.[4] There are two main factors in play here: topography development[5,6] and ion-beam-induced material alteration.[4,7,8] The latter issue is virtually solved by the introduction of large gas cluster ion beams (GCIB).[9−11] The topography development problem can be mitigated by sample rotation.[5] However, this approach limits analysis to depth dimension only because lateral spatial information is averaged out.

One possible source of topography development during ion irradiation is so-called spontaneous pattern formation where self-organized nanoscale ripples appear on the surface of the sample during the bombardment.[12,13] Over the years, there has been a substantial theoretical effort to develop models capable of qualitative and quantitative prediction of the surface evolution.[12−21] However, all available models have two main drawbacks concerning depth profiling with cluster projectiles. One is that none of these models have been applied to this type of projectiles or organic samples. All theoretical and almost all experimental research has been done with monatomic projectiles and inorganic samples. Only few experiments with cluster projectiles have been performed so far.[22−25] Another problem is that proposed theoretical models have a complicated mathematical formulation, which makes it difficult to develop adequate physical intuition regarding the phenomenon in question. Without proper understanding, countering the emergence of undesirable surface roughness during depth profiling is difficult.

In this manuscript, a simple model, based on a concept of mass transfer, is proposed to predict the conditions favorable for the formation of ripples on the solid surfaces bombarded by cluster projectiles. The unique beauty of this model is that, despite its simplicity, it can predict these conditions with good accuracy. Furthermore, it makes it easy to comprehend why surface roughness, which we equate to ripple formation, will increase or decrease under given experimental conditions.

SIMULATION DETAILS

The molecular dynamics computer simulations are used to model the effect of argon cluster bombardment of gold and silicon samples. General information about MD simulations can be found elsewhere.[26] Briefly, the motion of particles is determined by integrating Hamilton's equations of motion. Forces among particles are described by following potentials: the Lennard-Jones potential splined with KrC to accurately

Received: March 20, 2020
Accepted: April 21, 2020
Published: April 21, 2020

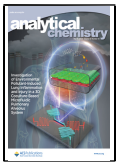

https://dx.doi.org/10.1021/acs.analchem.0c01219
Anal. Chem. 2020, 92, 7349−7353

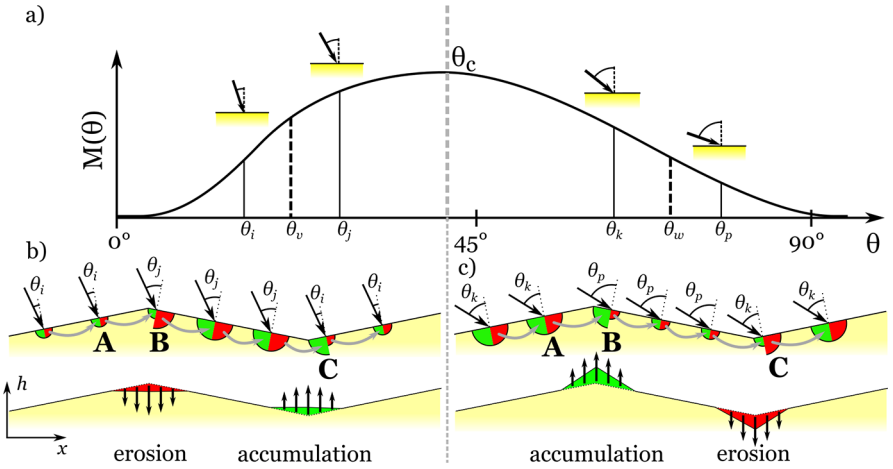

Figure 1. (a) Idealized effect of the incidence angle θ on the mass transfer function $M(\theta)$ for a bombardment by cluster projectiles and schematic visualizations of the effect of mass transfer on the sample topography in regions where $M(\theta)$ increases (b) or decreases (c) with θ. Green and red quarters represent the global mass inflow and outflow for a given node, respectively. Black tilted arrows represent directions of the impacting projectiles, and the symbols, θ_i, θ_j, θ_k, θ_p, describe local incidence angles. The global incidence angles are θ_v and θ_w.

describe high energy collisions is used to describe Ar−Ar interactions.[27] The Tersoff potential splined at a short distance with ZBL potential[28] is used to describe forces between Si atoms,[29] while EAM force field is used for Au atoms.[30,31] Finally, the ZBL potential is used to represent collisions between Ar−Au and Ar−Si atoms.[28] The simulations are performed with the LAMMPS code.[32]

The values of the mass transfer function M(theta) for different projectile parameters (kinetic energy, incidence angle) are extracted from MD trajectories. The divide and conquer approach developed for modeling depth profiling is used. This approach has been described in detail previously.[33,34] Briefly, a master sample is prepared as a cuboid with periodic boundary conditions imposed in x and y directions. The size of the master sample for silicon and gold equals to 40 × 40 × 30 nm and 42 × 42 × 32 nm, respectively. These samples contain 2.45 and 3.4 million atoms, respectively. Then, an impact point on the surface is selected randomly. A hemispherical region with a radius of 19 nm centered at this impact point is subsequently cut out from the master sample and used to simulate an impact of an Ar_{3000} cluster with a given kinetic energy and incident angle for 25 ps. The sample is subsequently quenched for 10 ps in order to maintain the desired temperature; it was equal to 0 K in the present study. After each simulation, all sputtered atoms are removed, the mass transfer function is calculated, and the remaining (nonsputtered) atoms are reinserted into the master sample. Subsequently, a new point of impact is randomly selected, and the cycle is repeated. For each combination of the kinetic energy and incident angle, a series of 50 simulations are performed, which corresponds to a fluence of approximately 3 × 10^{12} impacts/cm^2, and the final value of the mass transfer function is calculated as an average. Four test studies corresponding to the incidence angles of 30°, 35°, 45°, and 50° are performed on a silicon sample with a 10 times larger number of impacts to probe the effect of the projectile fluence on the mass transfer function dependence on the angle of incidence. While the amplitude of this dependence varies with the number of impacts, its shape (position of maximum) remained the same. Repetitive bombardment setup has been chosen to avoid strain introduced by a single impact.

The effect of projectile parameters (kinetic energy, incidence angle) on mass transfer can be obtained from molecular dynamics simulations. The mass transfer function is defined as

$$M = \sum_i V dx_i \tag{1}$$

where V is the volume occupied by an individual atom, dx_i is the displacement of the ith atom in the x-direction caused by the projectile impact, where the x-direction is the azimuthal direction of the incoming projectile, as proposed in ref 19. The ion beam density at the bombarded surface decreases with the angle of incidence θ due to the increase of the ion beam spot size on the irradiated surface. To account for this phenomenon, the results from the MD simulations should be normalized by the following formula:

$$M(\theta) = M_{MD}(\theta)\cos(\theta) \tag{2}$$

where $M(\theta)$ is the angle-dependent mass transfer function, and $M_{MD}(\theta)$ is the mass transfer calculated from the molecular dynamics simulations.

RESULTS AND DISCUSSION

The process of sputtering is believed to have a minor effect on the ripple formation during cluster projectile bombardment.[35,36] It is postulated that the mass transfer stimulated by impact of a projectile is of critical importance in this case.[35−37] In order to understand its influence, we begin by posing a question: what effect will a mass transfer near a surface have on its topography? To answer this question, we introduce a simple two-dimensional model, where the surface is represented by a set of discrete nodes, as shown in Figure 1. The coordinate system in this model is selected in such a way that the azimuthal direction of the ion beam is the x-axis, as depicted in Figure 1. Incoming projectiles are directed toward the macroscopic surface at the same global angle of incidence. This angle is equivalent to the experimental incidence angle. However, the global incidence angle usually does not represent the actual angle of incidence at a given node, because the real surface is never flat. In real samples, the local incidence angle should be defined relative to the surface normal at the point of projectile impact. It depends on the global angle of incidence

https://dx.doi.org/10.1021/acs.analchem.0c01219
Anal. Chem. 2020, 92, 7349−7353

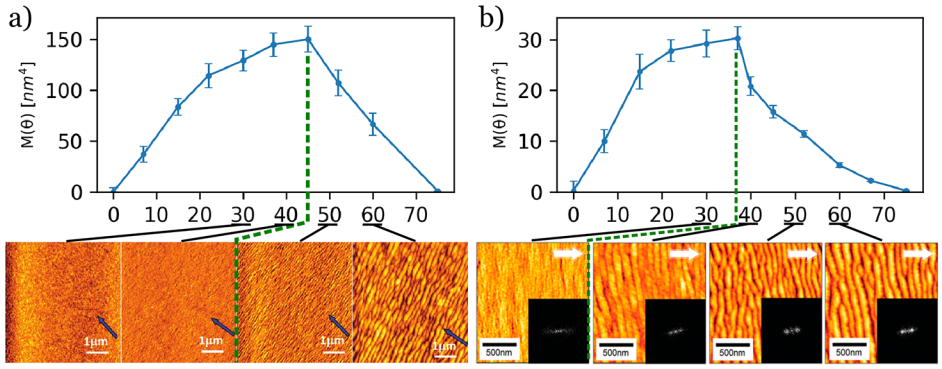

Figure 2. Angle-dependent mass transfer functions for (a) silicon and (b) gold samples sputtered by 30 keV Ar_{3000}. The AFM images show experimentally measured topography of the sample[23,24] at respective angles. The dashed green line depicts a location where the smoothing/roughening transition should be observed under reasoning presented in the text. The AFM images are reproduced with permission from refs 23 and 24 and are licensed under a Creative Commons Attribution (CC BY) license.

and the local surface inclination. The magnitude of these effects is proportional to the inclination of the $M(\theta)$ function for a given global incidence angle, so, for the cases where a plateau is reached, the mass redistribution will not influence surface topography.

After the projectile impact, the matter is transferred from one node to another. Our model is based on global mass transfer along the x-axis. For a cluster projectile impact at a flat surface along the surface normal, the same amount of material is transferred, on average, to the left and right neighbors of the bombarded node.[35,36] Therefore, from the point of view of a global mass transfer along the x-axis, the resulting mass transfer is zero. For the off-normal angle of incidence, the mass is transferred along an azimuth of the incoming beam.[36] The global mass transfer is no longer zero along the x-axis. The amount of mass transferred from a bombarded node increases initially with an increase of global incidence angle. However, the mass transfer must drop eventually, because no mass is transferred for the 90° incidence angle since the projectile never hits the sample. Based on these considerations, the value of the mass transfer function at a given node $M(\theta)$ should depend on the local angle of incidence θ, as shown in Figure 1a. There is a specific angle θ_c, which will be called a critical angle, where $M(\theta)$ has a maximum. This angle separates two regions, where $M(\theta)$ increases and decreases with the incidence angle.

Three possible surface morphologies should be considered to investigate the temporal evolution of the bombarded surface. The surface can be flat, convex (hill), or concave (hole), near a point of projectile impact. An example of a surface exhibiting all these cases is shown in Figure1b,c. The total amount of material transferred into and outside a given node is depicted as radii of the quarter-circles. Green and red quarters represent the mass inflow and outflow for a given node, respectively. For the off-normal incidence, the mass is transferred in the x-direction. In our model, this means that for a given node, the mass inflow occurs only from a node on the left, while the material is moved to the node on the right. A flat section of a surface represented by node A in Figure 1b,c is the simplest situation to discuss. In this case, the local angle of incidence at nodes A-1 and A is identical. As a result, the amount of material incoming and outcoming from node A is the same, as represented by quarters of the equal radii. Consequently, the height of node A is not affected relative to its neighbors, and the morphology does not change at this point. The situation is different for convex and concave surfaces represented by nodes B and C, respectively. In the case of a convex surface, the local incidence angle θ_j or θ_p at node B is larger than the local incidence angle θ_i or θ_k at node B-1. The opposite situation occurs for node C.

The final mass balance at nodes B and C depends on the shape of the $M(\theta)$ function. In the case where, for a given global incidence angle, $M(\theta)$ increases with θ, as depicted in Figure 1b, the mass inflow from the node B-1 is smaller than the outflow from node B, because $\theta_j > \theta_i$, therefore, $M(\theta_j) > M(\theta_i)$. The mass is removed, and the height of node B decreases, as indicated by downward-pointing vertical arrows. For a concave surface (node C), the situation is the opposite. More mass is transferred into node C than removed from it. As a result, the depth of this depression decreases. Considering both these effects, the global surface roughness will decrease for the impacts presented in Figure 1b.

Similar reasoning can be applied for the impact conditions where the $M(\theta)$ function decreases with θ. This case is depicted in Figure 1c. However, now the conclusions will be opposite to the situation shown in Figure 1b. While the relationship between θ_p and θ_k remains the same, that is, $\theta_p > \theta_k$, now $M(\theta_p) < M(\theta_k)$. Therefore, the global transfer to node B in Figure 1c is positive, while the mass is removed from node C. As a result, the elevation of the hill increases while the depression becomes more profound, which leads to an increase of the surface roughness. It is evident that the incidence angle corresponding to the maximum of the $M(\theta)$ function separates the surface smoothing and roughening regimes.

Experimental results describing the effect of the incidence angle on the ripple formation during the Ar_{3000} bombardment of silicon and gold surfaces[23,24] are used to verify the predictions of the proposed model. The shapes of the mass transfer functions calculated from molecular dynamics (MD) computer simulations are shown in Figure 2. The AFM images presenting experimentally measured topography of the sample at respective global incidence angles are shown below the graphs of individual $M(\theta)$ function. The experimental data show that the ripples begin to form above 40° and 30° at silicon and gold surfaces, respectively. The critical angles obtained from the calculated $M(\theta)$ functions for the same systems are 45° and 40°, respectively. It is evident that the transition from a smooth to a rough surface correlates very well with the value of the critical angle. This agreement proves that our model, regardless of its simplicity, is working correctly and

https://dx.doi.org/10.1021/acs.analchem.0c01219
Anal. Chem. 2020, 92, 7349−7353

corroborates the hypothesis that the mass transfer is predominantly responsible for an angle-dependent roughening/smoothing phenomenon during cluster projectile bombardment.

So far, only the effect of the incidence angle on the surface roughness was discussed. However, the kinetic energy of cluster projectiles may also influence the surface roughness. In fact, it has been shown that, at very low energies per atom, ripples appear in organic samples bombarded by gas cluster projectiles.[25] This process leads to fast degradation of the depth resolution with depth.[6,25] The problem was eliminated by increasing the projectile kinetic energy (energy per projectile atom). Unfortunately, the RMS roughness has not been directly measured in that paper.[25] Nevertheless, is has been established that the buildup of the surface roughness is the main factor limiting the achievable depth resolution.[6,11] Therefore, a possibility to achieve a better depth resolution indicates that the surface roughness must decrease with the increase of the kinetic energy per atom.

Angle-dependent mass transfer functions calculated for several kinetic energies of Ar_{3000} projectiles, bombarding the silicon surface, are shown in Figure 3 to probe the effect of the primary kinetic energy. Silicon is very different from the systems investigated in ref 25 where organic multilayers were analyzed. Therefore, no quantitative agreement between theoretical and experimental data can be expected. Nevertheless, similar trends should be observed in both these studies. It is evident that the value of the critical angle, which separates smoothing from roughening conditions, indeed shifts toward larger incidence angles with the increase of the projectile kinetic energy. It is expected, therefore, that at low projectile kinetic energy, the critical angle is below the incidence angle used in the experiment (45°), and the surface will be roughened. However, when kinetic energy is increased, the value of the critical angle θ_c shifts toward larger values, leading to a decrease of roughness due to the elimination of ripple formation.

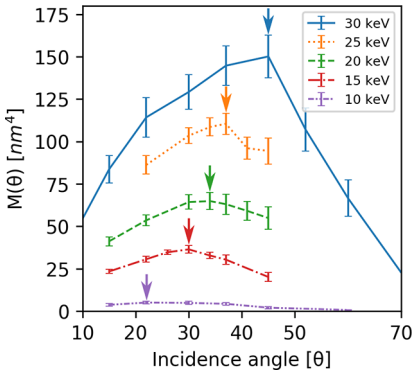

Figure 3. Angle-dependent mass transfer functions for silicon, bombarded by Ar_{3000} with different kinetic energies. For each incidence energy, the location of the maximum is highlighted by an arrow.

CONCLUSION

We have shown that ripple formation during cluster ion beam irradiation, which we equate to surface roughening, can be explained by impact-induced mass transfer with a simple and intuitive model. The main conclusion from our model is that the transition between smoothing and roughening regimes can be explained by the location of a maximum, called the critical angle, of an angle-dependent mass transfer function. If the incidence angle is lower than the critical angle, the mass transfer will have a smoothening effect, and if it is higher, the roughness will increase. Due to the nature of this function, the location of the maximum is expected to be around 45°. This finding has substantial practical importance because the incidence angle of a sputtering beam is 45° in a majority of commercially available apparatuses. We suggest that shifting the incidence angle closer to the surface normal by even a few degrees will have a beneficial impact on the quality of acquired depth profiles. Furthermore, we have shown that the increase of the cluster impact energy shifts the critical angle toward larger values. This observation suggests that the roughening problem, for some cases, can be resolved by increasing the kinetic energy of the beam. Finally, it should be mentioned that the proposed model works both for inorganic and organic samples. In this paper, we have focused on inorganic materials because results discussing the effect of the angle of incidence on the ripple formation are only available in the literature for such samples. We need such results to validate the predictions of our model. However, it should also be emphasized that our model can only be used to predict the onset of ripple formation during surface bombardment by cluster projectiles. Both the experimental results and computer simulations show that for these projectiles process of mass transfer prevails over sputtering.[23,24,34,36] As a result, sputtering can be ignored as it was done in our model. A similar approach cannot be applied to atomic missiles for which mass transport is much smaller due to the significantly smaller projectile size and momentum. Both the existing theories and experimental data indicate that the effect of sputtering cannot be ignored for these projectiles.[12−21]

AUTHOR INFORMATION

Corresponding Author

Zbigniew Postawa − *Smoluchowski Institute of Physics, Jagiellonian University, 30-348 Kraków, Poland;* orcid.org/0000-0002-7643-5911; Email: zbigniew.postawa@uj.edu.pl

Authors

Dawid Maciążek − *Smoluchowski Institute of Physics, Jagiellonian University, 30-348 Kraków, Poland*

Micha Kański − *Smoluchowski Institute of Physics, Jagiellonian University, 30-348 Kraków, Poland*

Complete contact information is available at: https://pubs.acs.org/10.1021/acs.analchem.0c01219

Notes

The authors declare no competing financial interest.

ACKNOWLEDGMENTS

This work was supported by the Polish National Science Center Program No. 2019/33/B/ST4/01778. MD simulations were performed at the PLGrid Infrastructure.

REFERENCES

(1) Fletcher, J. S. *Biointerphases* **2015**, *10*, 018902.
(2) McGettrick, J. D.; Speller, E.; Li, Z.; Tsoi, W. C.; Durrant, J. R.; Watson, T. *Org. Electron.* **2017**, *49*, 85−93.
(3) Hourani, W.; Gorbenko, V.; Barnes, J. P.; Guedj, C.; Cipro, R.; Moeyaert, J.; David, S.; Bassani, F.; Baron, T.; Martinez, E. *J. Electron Spectrosc. Relat. Phenom.* **2016**, *213*, 1−10.

(4) Wucher, A.; Cheng, J.; Winograd, N. *J. Phys. Chem. C* **2008**, *112*, 16550−16555.
(5) Sjovall, P.; Rading, D.; Ray, S.; Yang, L.; Shard, A. G. *J. Phys. Chem. B* **2010**, *114*, 769−774.
(6) Maciazek, D.; Paruch, R. J.; Postawa, Z.; Garrison, B. J. *J. Phys. Chem. C* **2016**, *120*, 25473−25480.
(7) Cheng, J.; Wucher, A.; Winograd, N. *J. Phys. Chem. B* **2006**, *110*, 8329−8336.
(8) Shard, A. G.; Green, F. M.; Brewer, P. J.; Seah, M. P.; Gilmore, I. S. *J. Phys. Chem. B* **2008**, *112*, 2596−2605.
(9) Ninomiya, S.; Ichiki, K.; Yamada, H.; Nakata, Y.; Seki, T.; Aoki, T.; Matsuo, J. *Rapid Commun. Mass Spectrom.* **2009**, *23*, 1601−1606.
(10) Mahoney, C. M. *Cluster Secondary Ion Mass Spectrometry: Principles and Applications*; Wiley: Hoboken, NJ, 2013.
(11) Winograd, N. *Annu. Rev. Anal. Chem.* **2018**, *11*, 29−48. and references therein.
(12) Chan, W. L.; Chason, E. *J. Appl. Phys.* **2007**, *101*, 121301. and references therein.
(13) Norris, S. A.; Aziz, M. J. *Appl. Phys. Rev.* **2019**, *6*, 011311. and references therein.
(14) Bradley, R. M.; Harper, J. M. E. *J. Vac. Sci. Technol., A* **1988**, *6*, 2390−2395.
(15) Makeev, M. A.; Cuerno, R.; Barabasi, A. L. *Nucl. Instrum. Methods Phys. Res., Sect. B* **2002**, *197*, 185−227.
(16) Aste, T.; Valbusa, U. *New J. Phys.* **2005**, *7*, 122.
(17) Munoz-Garcia, J.; Cuerno, R.; Castro, M. *Phys. Rev. B: Condens. Matter Mater. Phys.* **2008**, *78*, 205408.
(18) Chini, T. K.; Datta, D. P.; Bhattacharyya, S. R. *J. Phys.: Condens. Matter* **2009**, *21*, 224004.
(19) Norris, S. A.; Brenner, M. P.; Aziz, M. J. *J. Phys.: Condens. Matter* **2009**, *21*, 224017.
(20) Norris, S. A.; Samela, J.; Bukonte, L.; Backman, M.; Djurabekova, F.; Nordlund, K.; Madi, C. S.; Brenner, M. P.; Aziz, M. J. *Nat. Commun.* **2011**, *2*, 276.
(21) Norris, S. A.; Samela, J.; Vestberg, M.; Nordlund, K.; Aziz, M. J. *Nucl. Instrum. Methods Phys. Res., Sect. B* **2014**, *318*, 245−252.
(22) Toyoda, N.; Mashita, T.; Yamada, I. *Nucl. Instrum. Methods Phys. Res., Sect. B* **2005**, *232*, 212−216.
(23) Tilakaratne, B. P.; Chen, Q. Y.; Chu, W. K. *Materials* **2017**, *10*, 1056.
(24) Lozano, O.; Chen, Q. Y.; Tilakaratne, B. P.; Seo, H. W.; Wang, X. M.; Wadekar, P. V.; Chinta, P. V.; Tu, L. W.; Ho, N. J.; Wijesundera, D.; Chu, W. K. *AIP Adv.* **2013**, *3*, 062107.
(25) Niehuis, E.; Mollers, R.; Rading, D.; Cramer, H.-G.; Kersting, R. *Surf. Interface Anal.* **2013**, *45*, 158−162.
(26) Garrison, B. J.; Postawa, Z. *Mass Spectrom. Rev.* **2008**, *27*, 289−315. and references therein.
(27) Aziz, R. A.; Slaman, M. J. *Mol. Phys.* **1986**, *58*, 679−697.
(28) Ziegler, J. F.; Biersack, J. P.; Littmark, U. *The Stopping and Range of Ions in Matter*; Pergamon: New York, 1985.
(29) Tersoff, J. *Phys. Rev. B: Condens. Matter Mater. Phys.* **1989**, *39*, 5566−5568.
(30) Daw, M. S.; Baskes, M. I. *Phys. Rev. B: Condens. Matter Mater. Phys.* **1984**, *29*, 6443−6453.
(31) Foiles, S. M.; Baskes, M. I.; Daw, M. S. *Phys. Rev. B: Condens. Matter Mater. Phys.* **1986**, *33*, 7983−7991.
(32) Plimpton, S. *J. Comput. Phys.* **1995**, *117*, 1−19.
(33) Russo, M. F.; Postawa, Z.; Garrison, B. J. *J. Phys. Chem. C* **2009**, *113*, 3270−3276.
(34) Paruch, R.; Rzeznik, L.; Russo, M. F.; Garrison, B. J.; Postawa, Z. *J. Phys. Chem. C* **2010**, *114*, 5532−5539.
(35) Postawa, Z.; Czerwinski, B.; Szewczyk, M.; Smiley, E. J.; Winograd, N.; Garrison, B. J. *J. Phys. Chem. B* **2004**, *108*, 7831−7838.
(36) Paruch, R. J.; Postawa, Z.; Wucher, A.; Garrison, B. J. *J. Phys. Chem. C* **2012**, *116*, 1042−1051.
(37) Carter, G.; Vishnyakov, V. *Phys. Rev. B: Condens. Matter Mater. Phys.* **1996**, *54*, 17647−17653.

https://dx.doi.org/10.1021/acs.analchem.0c01219
Anal. Chem. 2020, 92, 7349−7353